
Chapter 1

Sensor-based Motion Control of Autonomous Underwater Vehicles, Part II: Robust Motion Control Strategies

*Charalampos P. Bechlioulis¹, Shahab Heshmati-alamdar¹,
George C. Karras¹, Panos Marantos¹ and Kostas J.
Kyriakopoulos¹*

1.1 Introduction

During the last decades, underwater robotic vehicles have been widely used in a variety of marine activities such as monitoring and inspection, surveillance of underwater facilities, oceanography. In most of these cases, the vehicles operate under the influence of strong external disturbances caused from ocean currents and waves. Moreover, the vehicle's dynamic parameters are likely to change, because different types of sensors and tools are utilized, depending on the requirements of each mission, for the AUV state estimation as well as the perception of the environment. Furthermore, the problem becomes much more intense especially when the vehicles are underactuated. Thus, the motion control scheme of an AUV should: i) be robust against external disturbances, ii) comply with the kinematic constraints of the vehicle and iii) up to a certain extend, independent from the vehicle's dynamics. Additionally, the aforementioned applications require the underwater robot to operate under various constraints and increased level of autonomy, in terms of energy consumption and endurance. Thus, recent research directions point towards the development of motion control strategies that are able to handle complex missions under operational constraints with reduced energy requirements.

The motion control problem for autonomous underwater vehicles has been an active research field for the past two decades and continues to pose considerable challenges to control designers especially when the vehicles exhibit large model uncertainty and are affected by environmental disturbances. A typical motion control problem is trajectory tracking which is concerned with the design of control laws that force a vehicle to reach and follow a reference trajectory. Classical approaches

¹School of Mechanical Engineering, Control Systems Lab, National Technical University of Athens, Greece {chmpechl, shahab, karrasg, marantos, kkyria}@mail.ntua.gr

2 Autonomous Underwater Vehicles: Design and Practice

such as local linearization and input-output decoupling have been used in the past to design tracking controllers for underactuated vehicles [1]. Nevertheless, the aforementioned methods yielded poor closed loop performance and the results were local, around only certain selected operating points. Alternative approaches involved output feedback linearization combined with PID control, linear quadratic optimal control and H_∞ control [2], which, however, was not always possible. Finally, based on a combined approach involving Lyapunov theory and the backstepping technique various nonlinear model-based trajectory tracking controllers have been reported during the last two decades [3–5]. However, these schemes demand a very accurate knowledge of the vehicle dynamic parameters which in most cases is quite difficult to obtain, and despite the recent progress in the tracking control for underwater vehicles, certain issues still remain open. Notice that even in case the actual vehicle model is considered accurately known, external disturbances affect severely the tracking performance thus making the problem of guaranteeing prescribed performance difficult or impossible in certain situations.

In general, the motion control of underwater vehicles is a highly nonlinear problem, where multiple input and state constraints are imposed to the system. Investigating the corresponding literature, it can be concluded that in most research works the input (generalized body forces/torques or thrust) and the state (3D obstacles, velocities) constraints are not considered. Hence, Nonlinear Model Predictive Control (NMPC) [6], can be considered an ideal approach for complex underwater missions, as it is able to combine motion planning, obstacle avoidance and workspace restrictions, while handling efficiently input and state constraints. The Model Predictive Control (MPC) has been already used in underwater motion planning. For instance, in order to optimize saw-tooth paths for an Autonomous Underwater Vehicle (AUV), an MPC scheme with a least squares cost function is presented in [7]. Interesting results including estimated ocean wave profiles into an NMPC scheme, with an emphasis on real-time execution are presented in [8]. However, the effects of noise and disturbances are not theoretically considered, but instead are demonstrated through simulation testing. In addition, an MPC approach with reduced dynamic model is presented in [9], where simplified linear models for the vertical and horizontal directions were considered, in order to avoid computational complexity. In the aforementioned works, only the kinematic model of the vehicle is considered. Moreover, the validation of the proposed strategies was conducted via simulation tests. An early experimental result of a visually aided NMPC scheme for an underwater robotic system was presented in [10], where simple kinematic equations of the system was considered.

The first section of this chapter presents an NMPC strategy for underwater robotic vehicles operating under various constraints. The purpose of the controller is to guide the vehicle towards specific way points. Various constraints such as: obstacles, workspace boundaries, control input saturation as well as predefined upper bound of the vehicle velocity (requirements for several underwater tasks such as seabed inspection scenario, mosaicking) are considered during the control design. The proposed scheme incorporates the full dynamics of the vehicle in which the ocean currents are also involved. The controller is designed in order to find

the optimal thrusts required for minimizing the way point tracking error. Moreover, the control inputs calculated by the proposed approach are formulated in a way that the vehicle will exploit the ocean currents, when they are in favor of the way-point tracking mission, which results in reduced energy consumption by the thrusters.

In the second part of this chapter, novel position and trajectory tracking control schemes for Autonomous Underwater Vehicles are presented. The proposed controllers do not utilize the vehicle's dynamic model parameters and guarantees prescribed transient and steady state performance despite the presence of external disturbances and kinematic constraints for the case of underactuated vehicles. Moreover, through the appropriate selection of certain performance functions, the proposed scheme can also guarantee the satisfaction of motion and performance constraints imposed by the desired task.

1.2 Model Predictive Control for Underwater Vehicles

1.2.1 PRELIMINARIES and PROBLEM FORMULATION

1.2.1.1 Notation

In this work, the vectors are denoted with lower bold letters whereas the matrices by capital bold letters. We define as $\mathcal{B}(\mathbf{c}, r) = \{\mathbf{x} \in \mathbb{R}^3 : \|\mathbf{x} - \mathbf{c}\| \leq r\}$ the closed sphere with radius r and center \mathbf{c} . For a given set $A \subset \mathbb{R}^n$ we define as $\text{cl}(A)$, $\text{int}(A)$ and $\partial S = \text{cl}(A) \setminus \text{int}(A)$ its closure, interior and boundary, respectively.

1.2.1.2 Mathematical Modeling

The pose vector of the vehicle with respect to (w.r.t) the inertial frame \mathcal{I} is denoted by $\boldsymbol{\eta} = [\boldsymbol{\eta}_1^T \ \boldsymbol{\eta}_2^T]^\top \in \mathbb{R}^6$ including the position (i.e., $\boldsymbol{\eta}_1 = [x \ y \ z]^\top$) and orientation (i.e., $\boldsymbol{\eta}_2 = [\phi \ \theta \ \psi]^\top$) vectors. Moreover, the $\mathbf{v} = [\mathbf{v}_1^T \ \mathbf{v}_2^T]^\top \in \mathbb{R}^6$ is the velocity vector of the vehicle expressed in fixed-body frame \mathcal{V} and includes the linear (i.e., $\mathbf{v}_1 = [u \ v \ w]^\top$) and angular (i.e., $\mathbf{v}_2 = [p \ q \ r]^\top$) velocity vectors. In this section, we consider that the vehicle operates under the influence of bounded irrotational ocean currents w.r.t the inertial frame \mathcal{I} . An estimation of the ocean currents can be achieved by employing the data obtained from Naval Coastal Ocean Model (NCOM) [11] and Regional Ocean Model Systems (ROMS) [12] or by employing a locally and appropriate estimator [13]. In this spirit, we denote the bounded irrotational ocean current velocities w.r.t the inertial frame \mathcal{I} by $\mathbf{v}_c^{\mathcal{I}} = [(\mathbf{v}_{c_1}^{\mathcal{I}})^\top, \mathbf{0}_{1 \times 3}]^\top \in \mathbb{R}^6$ with $\mathbf{v}_{c_1}^{\mathcal{I}} = [u_c^{\mathcal{I}}, v_c^{\mathcal{I}}, w_c^{\mathcal{I}}]^\top$ to be the vector of linear velocity terms. Therefore, we can define the vehicle velocity vector relative to the water expressed in body frame \mathcal{V} as:

$$\mathbf{v}_r = \mathbf{v} - \mathbf{v}_c \quad (1.1)$$

Notice that the vector $\mathbf{v}_c = [u_c, v_c, w_c, \mathbf{0}_{1 \times 3}]^\top$ indicates the expression of the ocean currents with respect to the body frame \mathcal{V} . Without loss of generality, assuming that the current velocity is slowly varying with respect to the inertial frame (e.g,

$\frac{\partial \mathbf{v}_c^{\mathcal{I}}}{\partial t} \approx 0$), and the vehicle is operating at relative low speeds, the dynamic equations of the vehicle can be given as [14, eq:3.110-3.116]:

$$\dot{\boldsymbol{\eta}} = \mathbf{J}(\boldsymbol{\eta}) \mathbf{v}_r + \mathbf{v}_c^{\mathcal{I}} \quad (1.2a)$$

$$\mathbf{M} \dot{\mathbf{v}}_r + \mathbf{C}(\mathbf{v}_r) \mathbf{v}_r + \mathbf{D}(\mathbf{v}_r) \mathbf{v}_r + \mathbf{g}(\boldsymbol{\eta}) = \boldsymbol{\tau}_{\mathcal{V}} \quad (1.2b)$$

where $\boldsymbol{\tau}_{\mathcal{V}}$ is the total propulsion force/torque vector; \mathbf{M} is the inertial matrix; $\mathbf{C}(\mathbf{v}_r)$ represents coriolis and centrifugal terms; $\mathbf{D}(\mathbf{v}_r)$ models dissipative effects; $\mathbf{g}(\boldsymbol{\eta}) \in \mathbb{R}^6$ is the hydrostatic restoring force vector; and $\mathbf{J}(\boldsymbol{\eta})$ is the well known Jacobian matrix transforming the velocities from the body-fixed (\mathcal{V}) to the inertial (\mathcal{I}) frame.

Remark 1. *The transformation from ocean current velocity defined in the inertial frame \mathcal{I} (i.e., $\mathbf{v}_c^{\mathcal{I}}$) into body-fixed one (i.e., \mathbf{v}_c) is achieved using the transposed rotation matrix i.e, $\mathbf{v}_c = \mathbf{J}^T(\boldsymbol{\eta}) \mathbf{v}_c^{\mathcal{I}}$ (See [14]).*

Remark 2. *In (1.2), the total propulsion force/torque vector ($\boldsymbol{\tau}_{\mathcal{V}}$) is computed using the thruster allocator matrix. Thus, for the vehicle used in the section's experimental results (i.e., a 4 DoF Seabotix LBV150) we can define a new thrust vector $\boldsymbol{\tau} = [\tau_{p_o}, \tau_s, \tau_{v_e}, \tau_l]^T \in \mathbb{R}^4$ (notations p_o , s , v_e and l denote the Port (p_o), Starboard (s), Vertical (v_e), Lateral (l) directions respectively), and the appropriate thruster allocator matrix ($\mathbf{T}_A \in \mathbb{R}^{4 \times 4}$) such as:*

$$\boldsymbol{\tau}_{\mathcal{V}}^{LBV} = \mathbf{T}_A \boldsymbol{\tau}, \quad (1.3)$$

where $\boldsymbol{\tau}_{\mathcal{V}}^{LBV} [X, Y, Z, N]^T \in \mathbb{R}^4$.

Remark 3. *In the vehicle used in this work (i.e., a 4 DoF Seabotix LBV150), the angles ϕ , θ and angular velocities p and q are negligible and we can consider them to be equal to zero. Thus, from now on, the $\boldsymbol{\eta} = [x, y, z, \psi]$ and $\mathbf{v} = [u, v, w, r]$.*

1.2.1.3 Problem formulation

In this Section we formally address the problem under consideration:

Problem 1. *Given an underwater vehicle with dynamics as described in (1.2), design a robust feedback control law for the autonomous guidance towards a set of way-points $\boldsymbol{\eta}_i^d$, $i = \{1, \dots, n\}$, while guaranteeing the following specifications:*

- *Avoid the workspace boundaries and a limited set of obstacles within.*
- *Respect operational limitations in the form of state (e.g velocity bounds) and input (thrust saturation) constraints.*
- *The energy consumed from thrusters to be retained in a reduced level.*

1.2.2 METHODOLOGY

In this Section we present in detail the methodologies proposed in order to guide the vehicle towards a set of way-points a set of way-points $\boldsymbol{\eta}_i^d$, $i = \{1, \dots, n\}$.



Figure 1.1: Experimental setup and problem formulation: the purpose of the controller is to guide the vehicle inside a constrained workspace.

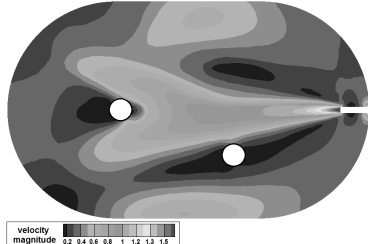


Figure 1.2: Distribution of the flow field inside the experimental water tank as computed by the CFD software presented in [15].

1.2.2.1 Geometry of Workspace

Consider an underwater robotic vehicle which operates inside the workspace $\mathcal{W} \subset \mathbb{R}^3$ with boundaries $\partial\mathcal{W} = \{\mathbf{p} \in \mathbb{R}^3 : \mathbf{p} \in \text{cl}(\mathcal{W}) \setminus \text{int}(\mathcal{W})\}$ and scattered obstacles located within. Without any loss of the generality, adopting spherical world representation [16], the robot and the obstacles are all modeled by spheres. In this spirit, let $\mathcal{B}(\boldsymbol{\eta}_1, \bar{r})$ to be a closed sphere that covers all the vehicle volume including main body and additional equipments. Moreover, the \mathcal{M} statics obstacles within the workspace are defined as closed spheres described by $\pi_m = \mathcal{B}(\mathbf{p}_{\pi_m}, r_{\pi_m})$, $m \in \{1, \dots, \mathcal{M}\}$, where $\mathbf{p}_{\pi_m} \in \mathbb{R}^3$ is the center and the $r_{\pi_m} > 0$ the radius of the obstacle π_m . Additionally, based on the property of spherical world [16], for each pair of obstacles $m, m' \in \{1, \dots, \mathcal{M}\}$ the following inequality holds:

$$\|\pi_m - \pi_{m'}\| > 2\bar{r} + r_{\pi_m} + r_{\pi_{m'}} \quad (1.4)$$

which intuitively means that the obstacles m and m' are disjoint in such a way that the entire volume of the vehicle can pass through the free space between them. Therefore, we assume that there exists a feasible trajectory $\boldsymbol{\eta}(t)$ for the vehicle that connects the initial configuration $\boldsymbol{\eta}(t_0)$ with $\boldsymbol{\eta}^d$.

1.2.2.2 Dynamical system

Due to the aforementioned assumptions and following standard simplifications due to symmetries in the mass configuration [14], the dynamic equation (1.2) for the vehicle under consideration, can be written in discrete-time form as:

$$\mathbf{x}_{k+1} = f(\mathbf{x}_k, \boldsymbol{\tau}_k) \Rightarrow \mathbf{x}_{k+1} = \mathbf{x}_k + \mathcal{A}(\mathbf{x}_k)dt + \mathcal{C}(\boldsymbol{\tau}_k)dt \quad (1.5)$$

6 Autonomous Underwater Vehicles: Design and Practice

where:

$$\mathcal{A}(\mathbf{x}_k) = \begin{bmatrix} u_{r_k} c \Psi_k - v_{r_k} s \Psi_k + u_c^{\mathcal{I}} \\ u_{r_k} s \Psi_k + v_{r_k} c \Psi_k + v_c^{\mathcal{I}} \\ w_{r_k} + w_c^{\mathcal{I}} \\ \frac{1}{m_{11}}(m_{22}v_{r_k}r_{r_k} + X_u|u_{r_k}|u_{r_k}|r_{r_k}) \\ \frac{1}{m_{22}}(-m_{11}u_{r_k}r_{r_k} + Y_v|v_{r_k}|Y_v|v_{r_k}|) \\ \frac{1}{m_{33}}(Z_ww_{r_k} + Z_w|w_{r_k}|w_{r_k}|r_{r_k}) \\ \frac{1}{m_{44}}((m_{11}-m_{22})u_{r_k}v_{r_k} + N_r|r_{r_k}|) \end{bmatrix}, \quad \mathcal{C}(\boldsymbol{\tau}_k) = \begin{bmatrix} \mathbf{0}_{4 \times 1} \\ \mathbf{T}_A \boldsymbol{\tau}_k \end{bmatrix}$$

with $c(\cdot) = \cos(\cdot)$, $s(\cdot) = \sin(\cdot)$ and $\mathbf{x}_k = [\boldsymbol{\eta}_k^\top, \mathbf{v}_{r_k}^\top]^\top = [x_k, y_k, z_k, \Psi_k, u_{r_k}, v_{r_k}, w_{r_k}, r_{r_k}]^\top \in \mathbb{R}^8$ denotes the state vector at the time-step k which includes the position and orientation of the vehicle with respect to the inertial frame \mathcal{I} and the relative linear and angular velocity of the vehicle with respect to the water. In addition, $m_{ii}, i = 1, \dots, 4$ are the mass terms including added mass, $X_u, Y_v, Z_w, N_r < 0$ are the linear drag terms, $X_{u|u|}, Y_{v|v|}, Z_{w|w|}, N_{r|r|} < 0$ are the quadratic drag terms, while dt denotes the sampling period. The control input of the system is $\boldsymbol{\tau}_k = [\tau_{p_k}, \tau_{s_k}, \tau_{v_k}, \tau_{l_k}]^\top \in \mathbb{R}^4$ consisting of the thrusters' forces.

1.2.2.3 Constraints

State Constraints:

We consider that the robot must avoid the obstacles and the workspace boundaries (test tank). Moreover, for the needs of several common underwater tasks (e.g., seabed inspection, mosaicking), the vehicle is required to move with relatively low speeds with upper bound denoted by the velocity vector $\mathbf{v}_p = [u_p \ v_p \ w_p \ r_p]^\top$. These requirements are captured by the state constraint set X of the system, given by:

$$\mathbf{x}_k \in X \subset \mathbb{R}^8 \quad (1.6)$$

which is formed by the following constraints:

$$u_p + v_p - |u_r + v_r| \geq 0 \quad (1.7a)$$

$$w_p - |w_r| \geq 0 \quad (1.7b)$$

$$r_p - |r_r| \geq 0 \quad (1.7c)$$

$$\mathcal{B}(\boldsymbol{\eta}_1(t), \bar{r}) \cap \{\mathcal{B}(\mathbf{p}_{\pi_m}, r_{\pi_m}) \cup \partial \mathcal{W}\} = \emptyset, m \in \{1, \dots, \mathcal{M}\} \quad (1.7d)$$

Input Constraints:

It is well known that the forces generated by the thrusters. Thus, we define the control constraint set T as follows:

$$\boldsymbol{\tau}_k = [\tau_{p_{ok}}, \tau_{s_k}, \tau_{v_{ek}}, \tau_{l_k}]^\top \in T \subseteq \mathbb{R}^4 \quad (1.8)$$

These constraints are of the form $|\tau_{p_{ok}}| \leq \bar{\tau}_{p_o}$, $|\tau_{s_k}| \leq \bar{\tau}_s$, $|\tau_{v_{ek}}| \leq \bar{\tau}_{v_e}$ and $|\tau_{l_k}| \leq \bar{\tau}_l$, therefore we get $\|\boldsymbol{\tau}_k\| \leq \bar{T}$ where $\bar{T} = (\tau_{p_o}^2 + \tau_s^2 + \tau_{v_e}^2 + \tau_l^2)^{\frac{1}{2}}$ and $\bar{\tau}_{p_o}, \bar{\tau}_s, \bar{\tau}_{v_e}, \bar{\tau}_l \in \mathbb{R}_{\geq 0}$.

1.2.2.4 Control Design

The control objective is to guide the regions around the waypoints $i = \{1, \dots, n\}$ that includes the desired state ${}^i\mathbf{x}^d \triangleq [({}^i\boldsymbol{\eta}^d)^\top, ({}^i\mathbf{v}_r^d)^\top]^\top = [x_d, {}^i y_d, {}^i z_d, {}^i \psi_d, {}^i u_d, {}^i v_d, {}^i w_d, {}^i r_d]^\top \in X$, while respecting the state constraints (1.7a)-(1.7d) as well as the input constraints (1.8). A predictive controller is employed in order to achieve this task. In particular, at a given time instant k , the NMPC is assigned to solve an Optimal Control Problem (OCP) with respect to a control sequence $\boldsymbol{\tau}_f(k) \triangleq [\boldsymbol{\tau}(k|k), \boldsymbol{\tau}(k+1|k), \dots, \boldsymbol{\tau}(k+N-1|k)]$, for a prediction horizon N . The OCP of the NMPC is given as follows:

$$\min_{\boldsymbol{\tau}_f(k)} J_N(\mathbf{x}_k, \boldsymbol{\tau}_f(k)) = \quad (1.9a)$$

$$\min_{\boldsymbol{\tau}_f(k)} \sum_{j=0}^{N-1} F(\hat{\mathbf{x}}(k+j|k), \boldsymbol{\tau}(k+j|k)) + E(\hat{\mathbf{x}}(k+N|k))$$

subject to:

$$\hat{\mathbf{x}}(k+j|k) \in X_j, \quad \forall j = 1, \dots, N-1, \quad (1.9b)$$

$$\boldsymbol{\tau}(k+j|k) \in T, \quad \forall j = 0, \dots, N-1, \quad (1.9c)$$

$$\hat{\mathbf{x}}(k+N|k) \in \mathcal{E}_f \quad (1.9d)$$

where \mathcal{E}_f is the terminal set and F and E are the running and terminal cost functions, respectively. At time instant k , the solution of the OCP (1.9a)-(1.9d) is providing an optimal control sequence, denoted as:

$$\boldsymbol{\tau}_f^*(k) = [\boldsymbol{\tau}(k|k), \boldsymbol{\tau}(k+1|k), \dots, \boldsymbol{\tau}(k+N-1|k)] \quad (1.10)$$

where the first control vector (i.e., $\boldsymbol{\tau}(k|k)$) is applied to the system. Notice we use the double subscript notation for the predicted state of system (1.5) inside the OCP of the NMPC:

$$\hat{\mathbf{x}}(k+j|k) = f(\hat{\mathbf{x}}(k+j-1|k), \boldsymbol{\tau}(k+j-1|k)) \quad (1.11)$$

where the vector $\hat{\mathbf{x}}(k+j|k)$ denotes the predicted state of the system (1.5) at sampling time $k+j$ with $j \in \mathbb{Z}_{\geq 0}$. The predicted state is based on the measurement of the state \mathbf{x}_k of the system at sampling time k (i.e., provided by onboard navigation system), while applying a sequence of control inputs $[\boldsymbol{\tau}(k|k), \boldsymbol{\tau}(k+1|k), \dots, \boldsymbol{\tau}(k+j-1|k)]$. It holds that $\hat{\mathbf{x}}(k|k) \equiv \mathbf{x}_k$. The cost function $F(\cdot)$, as well as the terminal cost $E(\cdot)$, are both of quadratic form, i.e., $F(\hat{\mathbf{x}}, \boldsymbol{\tau}) = \hat{\mathbf{x}}^\top Q \hat{\mathbf{x}} + \boldsymbol{\tau}^\top R \boldsymbol{\tau}$ and $E(\hat{\mathbf{x}}) = \hat{\mathbf{x}}^\top P \hat{\mathbf{x}}$, respectively, with P , Q and R being positive definite matrices. Particularly we define $Q = \text{diag}\{q_1, \dots, q_8\}$, $R = \text{diag}\{r_1, \dots, r_4\}$ and $P = \text{diag}\{p_1, \dots, p_8\}$.

1.2.3 EXPERIMENTAL RESULTS

This subsection demonstrates the efficacy of the proposed motion control scheme via a set of real-time experiments employing a small underwater robotic vehicle.

1.2.3.1 Setup

The experiments were carried out inside the *NTUA, Control Systems Lab* test tank, with dimensions $5m \times 3m \times 1.5m$ (Fig. 1.1). The bottom of the tank is covered by a custom-made poster with various visual features and markers. Two cylindrical objects with known position and dimensions are placed inside the tank and considered as static obstacles. The vehicle used in this work is a 4 DoFs Seabotix LBV, actuated in Surge, Sway, Heave and Yaw via a 4 thruster set configuration. The vehicle is equipped with a down-looking Sony PlayStation Eye camera, with 640×480 pixels at 30 frames per second (fps) enclosed in a waterproof housing. An underwater laser pointer projecting a green dot at the bottom of the test tank is rigidly attached on the vehicle with its axes aligned to the down-looking camera axis. The vehicle is also equipped with an *SBG IG – 500A AHRS*, delivering temperature-compensated 3D acceleration, angular velocity and orientation measurements at $100Hz$. The marker localization system is based on the *ArUco* library [17] and the overall state vector of the vehicle ($3D$ position, orientation, velocity) is available via a sensor fusion and state estimation module based on the Complementary Filter notion presented in our previous results [18]. The vehicle's dynamic parameters have been identified via a proper identification scheme. The software implementation of the proposed motion control scheme was conducted in C++ and Python under the Robot Operating System (ROS) [19]. The disturbances in the form of water currents, were induced

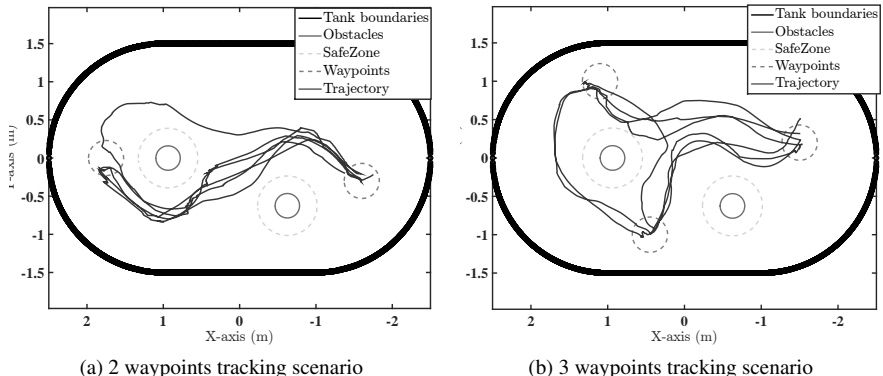


Figure 1.3: Vehicle trajectory in horizontal plane

using a *BTD150* thruster properly mounted inside the water tank. The generated flow field (i.e., assumed ocean current profile), was computed using a GPU-enabled Computational fluid Dynamics (CFD) software [15] developed in the Parallel CFD and Optimization Unit of the school of Mechanical Engineering of NTUA. The flow field distribution inside the water tank is depicted in Fig-1.2.

1.2.3.2 Results

In order to prove the efficacy of the proposed controller two experiments are presented (Scenario A and B). In both experiments, the objective is to follow a set of predefined waypoints while simultaneously avoid two static obstacles and respect

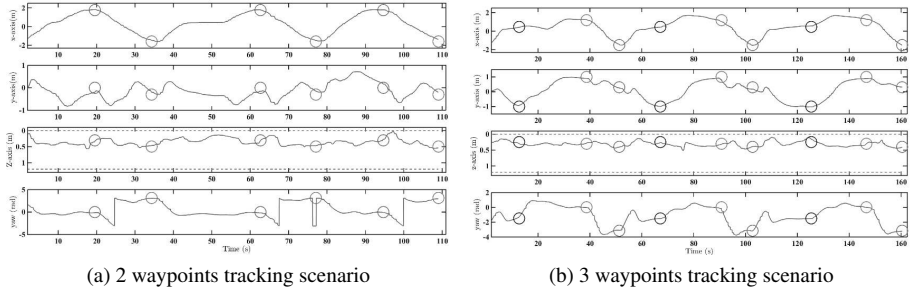
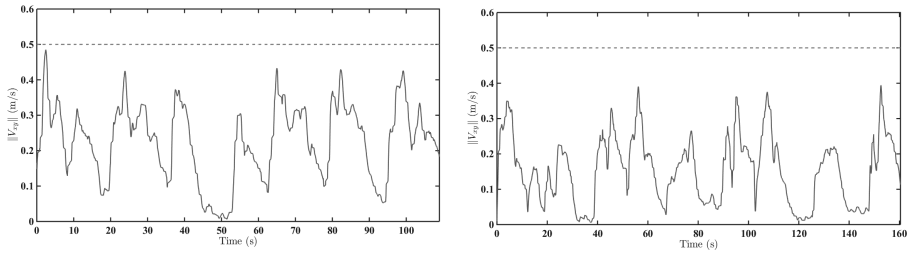


Figure 1.4: Vehicle vertical and angular motion

the workspace (test tank) boundaries. The location and geometry of the obstacles are considered known. More specific, the position of the obstacles w.r.t the Inertial Frame \mathcal{I} in $x - y$ plane is given by: $obs_1 = [-0.625, -0.625]$, $obs_2 = [0.9375, 0]$. The state constraints of the (1.7a)-(1.7d) which must be satisfied during all the experiments are analytically formulated as follows: i) The obstacles are cylinders (See Fig.1.1) with radius $r_{\pi_i} = 0.16m$, $i = \{1,2\}$ and are modeled together with the workspace boundaries according to the spherical world representations as consecutive spheres. ii) the radius of the sphere $\mathcal{B}(\boldsymbol{\eta}_1, \bar{r})$ which covers all the vehicle volume (i.e., main body and additional equipment) is defined as $\bar{r} = 0.3m$. However, for the clarity of presentation, we depict it as a safe zone around the obstacles where the vehicle center $\boldsymbol{\eta}_1$ (denoted by blue line See Fig.1.3a-Fig.1.3b) should not violated it. iii) the vertical position must be between $0 < z < 1.2 m$, iv) the vehicle's body velocity norm of (1.7a) $|u_r + v_r|$ (planar motion) must not exceed $0.5m/s$. v) heave velocity must be retained between $-0.25 < w_r < 0.25 m/s$. vi) yaw velocity must be retained between $-1 < r_y < 1 rad/s$. Moreover, each of the four thrusters

Figure 1.5: Vehicle body velocity norm $|u_r + v_r|$

must obey the following input constraint: $-12 < \tau_i < 12N$, $i = \{p_o, s, v_e, l\}$. The state and input constraints in the following figures are depicted in red dashed lines were applicable. At this point we should mention that each mission is considered as successful only if the vehicle performs the waypoint tracking three consecutive

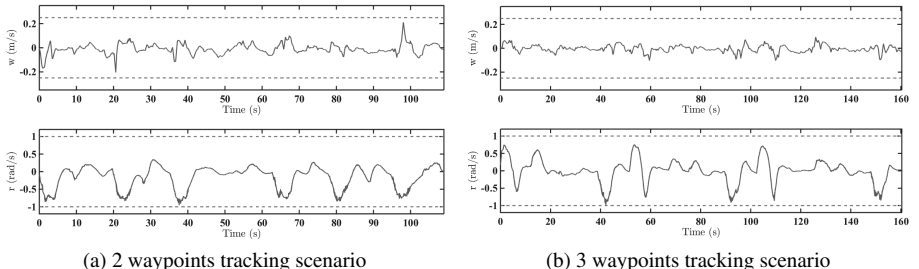


Figure 1.6: Vehicle heave and yaw velocities

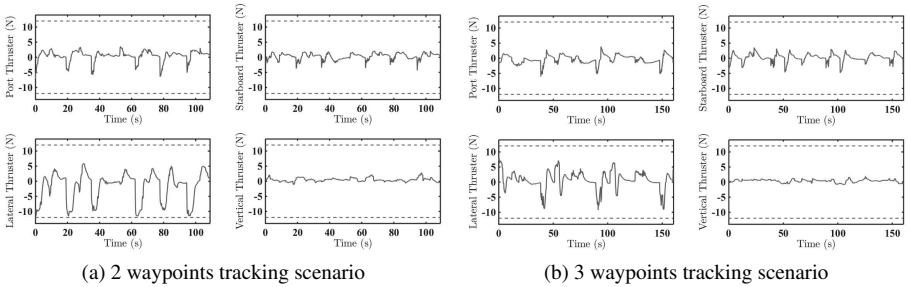


Figure 1.7: Thruster Commands

times, hence repeatability is proved. In all times the vehicle is under the influence of the water currents depicted in Fig 1.2.

Scenario A: Two Way Points Tracking. In this scenario the vehicle must travel via two waypoints which are placed at $\eta_1^d = [-1.6, -0.35, 0.45, 0]$, $\eta_2^d = [1.75, 0, 0.3, \pi]$ respectively. The three consecutive trajectories of the vehicle along the horizontal plane are depicted in Fig. 1.3a. It can be seen that the vehicle performs successfully the waypoint tracking while safely avoids the obstacles and the test tank boundaries. We observe that in one case the vehicle traveled from the second waypoint back to first one following a different trajectory. This can be explained by the fact that the MPC found a different optimal solution at the specific time frame, due to the unmodeled dynamics of the tether which significantly affect the vehicle motion. The vertical and angular motion of the vehicle are depicted in Fig. 1.4a where it can be seen that the state constraints are always satisfied. The vehicle is consider to reach each waypoint if it has entered a terminal region \mathcal{E}_f (i.e., spherical region of 0.3m and a offset of $\pm 0.15\text{rad}$) around the waypoint. These regions are depicted in circles in Fig. 1.3a and 1.4a. In Fig. 1.5a the body velocity norm in planar motion is depicted and the respective constraint is satisfied. The same stands for the heave and yaw velocities as shown in Fig. 1.6a. In Fig. 1.7a the vehicle's thruster input are shown. As it can be seen the input constraints are also satisfied.

Scenario B: Three Way Points Tracking. This scenario is similar to the previous one except that the vehicle must travel along 3 waypoints which makes the mission more challenging considering the narrow workspace. The locations of the three waypoints are given by: $\boldsymbol{\eta}_1^d = [-1.50m, 0.30m, 0.40m, -\frac{\pi}{2} rad]$, $\boldsymbol{\eta}_2^d = [0.45, -1, 0.25, 0]$, $\boldsymbol{\eta}_3^d = [1.2, 1, 0.3, -\pi]$. The three consecutive trajectories of the vehicle along the horizontal plane are depicted in Fig. 1.3b. Although this scenario is more complicated the vehicle again carries it out successfully. As it can be observed, the vehicle also in this mission follows different trajectories, for the same reasons explained in Scenario A. The vertical and angular motion of the vehicle are depicted in Fig. 1.4b, while in Fig. 1.5b the body velocity norm in planar motion is shown. The heave and yaw velocities are presented in Fig. 1.6b, while in Fig. 1.7b the vehicle's thruster inputs are shown. As it can be observed, the vehicle achieved all desired waypoints while simultaneously satisfied all respective state and input constraints.

1.3 Model-free Control for Underwater Vehicles

1.3.1 Fully Actuated Underwater Vehicles

1.3.1.1 AUV Kinematics and Dynamics

In this section, we consider a simplified 3D dynamic model (in surge, sway, heave and yaw) of an AUV in accordance to the standard underwater vehicle modeling properties [1]. The roll and pitch degrees of freedom are neglected for the clarity of the presentation. However, the stability of both degrees of freedom can be secured owing to their Input to State Stability (ISS) properties, without compromising the achieved results. In this respect, consider the vehicle modeled as a rigid body subject to external forces and torques. Let $\{I\}$ be an inertial coordinate frame and $\{B\}$ a body-fixed coordinate frame, whose origin O_B is located at the center of mass of the vehicle. Furthermore, let (x, y, z) be the position of O_B in $\{I\}$ and ψ denote the yaw angle. Let (u, v, w) be the longitudinal (surge), transverse (sway) and vertical (heave) velocities of O_B with respect to $\{I\}$ expressed in $\{B\}$ and r be the vehicle's angular speed (yaw) around the vertical axis. Thus, the kinematic equations of motion for the considered vehicle can be written as:

$$\dot{x} = u \cos \psi - v \sin \psi + \delta_x(t) \quad (1.12)$$

$$\dot{y} = u \sin \psi + v \cos \psi + \delta_y(t) \quad (1.13)$$

$$\dot{z} = w + \delta_z(t) \quad (1.14)$$

$$\dot{\psi} = r + \delta_\psi(t) \quad (1.15)$$

where $\delta_x(t)$, $\delta_y(t)$, $\delta_z(t)$, $\delta_\psi(t)$ denote bounded ocean currents. Neglecting the motion in roll and pitch, the simplified equations for the surge, sway, heave and yaw

can be written as:

$$m_u \dot{u} = m_v v r + X_{|u|u} |u| u + X + \delta_u(t) \quad (1.16)$$

$$m_v \dot{v} = -m_u u r + Y_{|v|v} |v| v + Y + \delta_v(t) \quad (1.17)$$

$$m_w \dot{w} = Z_{|w|w} |w| w + (W - B) + Z + \delta_w(t) \quad (1.18)$$

$$m_r \dot{r} = (m_u - m_v) u v + N_r r + N_{|r|r} |r| r + N + \delta_r(t) \quad (1.19)$$

where m_u , m_v , m_w , m_r denote the vehicle's mass, moment of inertia, added mass and moment of inertia terms, X_u , $X_{|u|u}$, Y_v , $Y_{|v|v}$, Z_w , $Z_{|w|w}$, N_r , $N_{|r|r}$ are negative hydrodynamic damping coefficients of first and second order, W and B are the vehicle weight and buoyancy respectively, $\delta_u(t)$, $\delta_v(t)$, $\delta_w(t)$, $\delta_r(t)$ denote bounded exogenous forces and torques acting on surge, sway, heave and around yaw owing to ocean waves and X , Y , Z , N denote the control input forces and torque respectively that are applied by the thrusters in order to produce the desired motion of the body fixed frame.

1.3.1.2 Control Scheme

Let $x_d(t)$, $y_d(t)$, $z_d(t)$ and $\psi_d(t)$ denote a desired smooth and bounded trajectory as well as yaw orientation respectively. The objective is to design a controller, without incorporating any information regarding the vehicle model, such that: a) it tracks the desired trajectory with the desired orientation via bounded closed loop signals and b) it achieves prescribed transient and steady state performance, despite the presence of exogenous disturbances representing ocean currents and waves.

Let us define the position errors:

$$e_x = x - x_d, e_y = y - y_d, e_z = z - z_d \quad (1.20)$$

as well as the orientation error:

$$e_\psi = \psi - \psi_d. \quad (1.21)$$

Given the desired trajectory $x_d(t)$, $y_d(t)$, $z_d(t)$ and orientation $\psi_d(t)$ as well as the position/orientation errors (1.20)-(1.21):

I. Kinematic Controller

Select the exponentially decaying position/orientation performance functions $\rho_x(t)$, $\rho_y(t)$, $\rho_z(t)$, $\rho_\psi(t)$ that i) satisfy:

a. $ e_x(0) < \rho_x(0)$	$0 < \rho_x(t)$	$0 < \lim_{t \rightarrow \infty} \rho_x(t)$
b. $ e_y(0) < \rho_y(0)$	$0 < \rho_y(t)$	$0 < \lim_{t \rightarrow \infty} \rho_y(t)$
c. $ e_z(0) < \rho_z(0)$	$0 < \rho_z(t)$	$0 < \lim_{t \rightarrow \infty} \rho_z(t)$
d. $ e_\psi(0) < \rho_\psi(0)$	$0 < \rho_\psi(t)$	$0 < \lim_{t \rightarrow \infty} \rho_\psi(t)$

and ii) incorporate the desired performance specifications regarding the steady state error and the speed of convergence; and design the desired velocities:

$$\begin{bmatrix} u_d \\ v_d \\ w_d \end{bmatrix} = \begin{bmatrix} \cos \psi & -\sin \psi & 0 \\ \sin \psi & \cos \psi & 0 \\ 0 & 0 & 1 \end{bmatrix}^{-1} \begin{bmatrix} -k_x \frac{e_x}{\rho_x(t)} \\ -k_y \frac{e_y}{\rho_y(t)} \\ -k_z \frac{e_z}{\rho_z(t)} \end{bmatrix} \quad (1.22)$$

$$r_d = -k_\psi \frac{e_\psi}{\rho_\psi(t)} \quad (1.23)$$

with positive control gains k_x, k_y, k_z, k_ψ .

II. Dynamic Controller

Select exponentially decreasing velocity performance functions $\rho_u(t), \rho_v(t), \rho_w(t), \rho_r(t)$ that satisfy:

a. $ u(0) - u_d(0) < \rho_u(0)$	$0 < \rho_u(t)$	$0 < \lim_{t \rightarrow \infty} \rho_u(t)$
b. $ v(0) - v_d(0) < \rho_v(0)$	$0 < \rho_v(t)$	$0 < \lim_{t \rightarrow \infty} \rho_v(t)$
c. $ w(0) - w_d(0) < \rho_w(0)$	$0 < \rho_w(t)$	$0 < \lim_{t \rightarrow \infty} \rho_w(t)$
d. $ r(0) - r_d(0) < \rho_r(0)$	$0 < \rho_r(t)$	$0 < \lim_{t \rightarrow \infty} \rho_r(t)$

and design the external forces in the surge, sway and heave as well as the external torque around yaw as:

$$X = -k_u \frac{u - u_d}{\rho_u(t)}, Y = -k_v \frac{u - u_d}{\rho_u(t)}, Z = -k_w \frac{w - w_d}{\rho_w(t)}, N = -k_r \frac{r - r_d}{\rho_r(t)} \quad (1.24)$$

with positive control gains k_u, k_v, k_w, k_r .

1.3.1.3 Experiments

To illustrate the performance of the proposed control scheme, two experimental procedures were carried out: a) navigation and stabilization to a specific configuration, b) meanders-like trajectory tracking. The experiments took place inside a water tank using the Girona500 AUV. A panel consisting of valves and handles located inside the pool was used as the visual target during the experiments and a navigation module was responsible for providing the state feedback to the closed loop system in both experiments. In order to create strong external disturbances to the system, a water jet mechanism was installed on the AUV 4 DoFs robotic manipulator. The water jet was installed on the second rotational DoF of the manipulator which was moving constantly in both experiments in order to create time-varying and multidirectional external disturbances, as shown in Fig. 1.9 and Fig. 1.12.

Navigation and Stabilization towards a specific configuration

In this experiment, the vehicle starts from an arbitrary initial configuration in order to navigate and stabilize towards a specific configuration (in front of a control panel). During the motion, the vehicle is constantly under the effect of time-varying and multidirectional external disturbances caused by the water jet mechanism. The required transient and steady state specifications, (that is, maximum steady state position errors 0.05m, maximum steady state orientation error 5° and

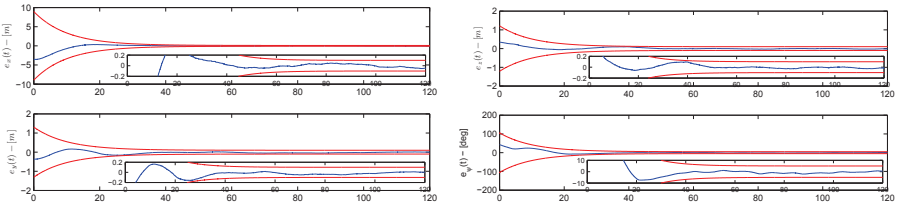


Figure 1.8: Tracking error evolution during navigation and stabilization towards a specific configuration. The red lines indicate the desired performance bounds. The blue lines indicate the evolution of $e_x(t)$, $e_y(t)$, $e_z(t)$ and $e_\psi(t)$

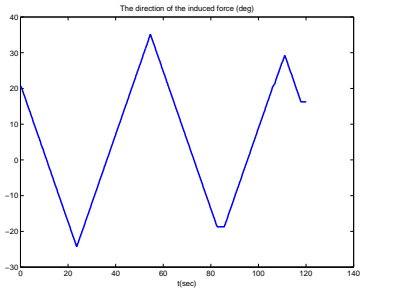


Figure 1.9: Direction of the external disturbance induced by the water jet during the navigation and stabilization towards a specific configuration.

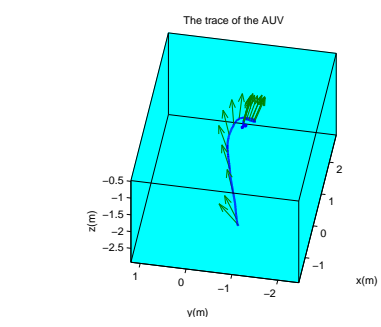


Figure 1.10: 3D trajectory of the AUV while performing navigation and stabilization towards a specific configuration.

exponential convergence $e^{-0.1t}$), are described by the following performance functions: $\rho_x(t) = (4.5 - 0.05)e^{-0.1t} + 0.05$, $\rho_y(t) = (3.0 - 0.05)e^{-0.1t} + 0.05$, $\rho_z(t) = (1 - 0.05)e^{-0.1t} + 0.05$, $\rho_\psi(t) = (85 - 5)e^{-0.1t} + 5$, $\rho_u(t) = (1 - 0.1)e^{-0.1t} + 0.1$, $\rho_v(t) = (1 - 0.1)e^{-0.1t} + 0.1$, $\rho_w(t) = (1 - 0.1)e^{-0.1t} + 0.1$, $\rho_r(t) = (1 - 0.1)e^{-0.1t} + 0.1$. Finally, the control gains were chosen as follows: $k_x = 1$, $k_y = 0.5$, $k_z = 0.5$, $k_\psi = 0.5$, $k_u = 15$, $k_v = 7.5$, $k_w = 15$, $k_r = 7.5$.

The tracking error evolution is depicted in Fig. 1.8. The red lines indicate the desired performance bounds and the blue lines indicate the evolution of the tracking errors $e_x(t)$, $e_y(t)$, $e_z(t)$ and $e_\psi(t)$ respectively. All the errors have met the transient and steady state specifications imposed by the previously selected performance functions. The 3D trajectory of the vehicle is shown in Fig. 1.10 in the blue line. As it can be seen from the results, the control objective has been achieved under the influence of external disturbances.

Meandrus-like Trajectory Tracking

In this experiment, the vehicle starts from an arbitrary initial configuration in order to perform a meandrus-like trajectory tracking under the effect of time-varying and multidirectional external disturbances. The required transient and steady state spec-

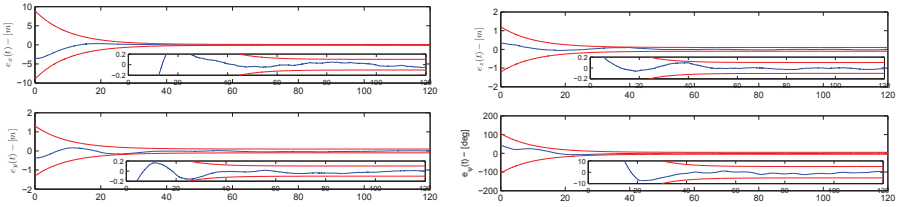


Figure 1.11: Tracking error evolution during meanders-like trajectory. The red lines indicate the desired performance bounds. The blue lines indicate the evolution of $e_x(t)$, $e_y(t)$, $e_z(t)$ and $e_\psi(t)$

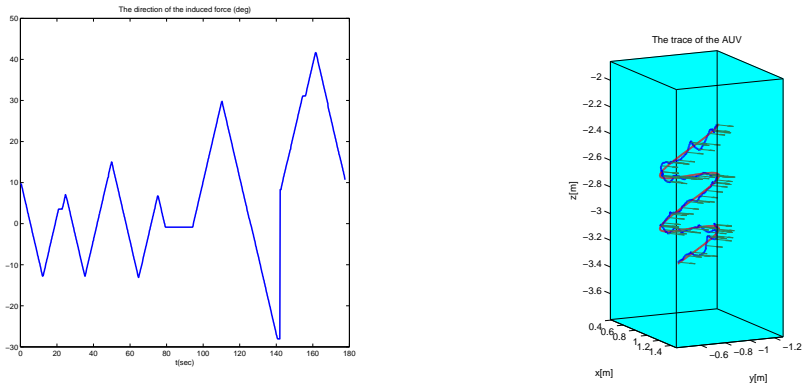


Figure 1.12: Direction of the external disturbance induced by the water jet during the meanders-like trajectory tracking.

Figure 1.13: 3D trajectory of the AUV while performing the meanders-like trajectory tracking.

ifications are the same with the previous experiment. Therefore, we employed the same performance functions and control gains in the control scheme.

The tracking error evolution during the steady state is depicted in Fig. 1.11. The red lines indicate the desired performance bounds and the blue lines indicate the evolution of the tracking errors $e_x(t)$, $e_y(t)$, $e_z(t)$ and $e_\psi(t)$ respectively. The 3D trajectory of the vehicle is shown in Fig. 1.13. The red line depicts the desired trajectory, while the blue one depicts the actual performed by the AUV. As it is demonstrated by the experiments and predicted from the theoretical analysis, the control objective has been achieved in the presence of external disturbances.

1.3.2 Underactuated Underwater Vehicles - Case I

A simplified 3D dynamic model of an underwater robotic vehicle is presented in this section and a rigorous formulation of the tracking problem of a desired trajectory is introduced. The vehicle has two identical rear thrusters, mounted symmetrically

with respect to its longitudinal axis as well as a thruster mounted along the vertical axis. The common and the differential action modes of the rear thrusters result in a force X along the vehicle's longitudinal axis and a torque N about its vertical axis, respectively, whereas the action of the vertical thruster results in a force Z along the corresponding axis. The aforementioned forces X , Z and torque N define the input control variables of the dynamic system. In this respect, the vehicle is underactuated since it lacks a lateral thruster. Finally, the roll and pitch degrees of freedom are neglected for the clarity of the presentation. However, both degrees of freedom are stable and do not affect the analysis.

1.3.2.1 Vehicle Kinematics and Dynamics

Consider an underactuated underwater vehicle modeled as a rigid body subject to external forces and torques. Let $\{I\}$ be an inertial coordinate frame and $\{B\}$ a body-fixed coordinate frame, whose origin O_B is located at the center of mass of the vehicle. Furthermore, let (x, y, z) be the position of O_B in $\{I\}$ and ψ denote the yaw angle. Let (u, v, w) be the longitudinal (surge), transverse (sway) and vertical (heave) velocities of O_B with respect to $\{I\}$ expressed in $\{B\}$ and r be the vehicle's angular speed (yaw) around the vertical axis. Hence, the kinematic equations of motion for the considered vehicle can be written as:

$$\dot{x} = u \cos \psi - v \sin \psi + \delta_x(t) \quad (1.25)$$

$$\dot{y} = u \sin \psi + v \cos \psi + \delta_y(t) \quad (1.26)$$

$$\dot{z} = w + \delta_z(t) \quad (1.27)$$

$$\dot{\psi} = r \quad (1.28)$$

where $\delta_x(t)$, $\delta_y(t)$, $\delta_z(t)$ denote bounded ocean currents. Neglecting the motion in roll and pitch, the simplified equations for the surge, sway, heave and yaw can be written as:

$$m_u \ddot{u} = m_v v r + X_{|u|u} |u| u + X + \delta_u(t) \quad (1.29)$$

$$m_v \ddot{v} = -m_u u r + Y_{|v|v} |v| v + \delta_v(t) \quad (1.30)$$

$$m_w \ddot{w} = Z_{|w|w} |w| w + Z + \delta_w(t) \quad (1.31)$$

$$m_r \ddot{r} = (m_u - m_v) u v + N_r r + N_{|r|r} |r| r + N + \delta_r(t) \quad (1.32)$$

where m_u , m_v , m_w , m_r denote the vehicle's mass, moment of inertia, added mass and moment of inertia terms, X_u , $X_{|u|u}$, Y_v , $Y_{|v|v}$, Z_w , $Z_{|w|w}$, N_r , $N_{|r|r}$ are negative hydrodynamic damping coefficients of first and second order, $\delta_u(t)$, $\delta_v(t)$, $\delta_w(t)$, $\delta_r(t)$ denote bounded exogenous forces and torques acting on surge, sway, heave, yaw owing to ocean waves and X , Z , N denote the control input forces and torque respectively that are applied by the thrusters in order to produce the desired motion of the body fixed frame. Finally, notice that there is no lateral thruster to control the sway motion. Hence, Eq. (1.30) is uncontrolled making thus (1.25)-(1.32) an underactuated dynamical system. It is important to stress that the dynamics of the sway velocity v must be explicitly taken into account since the presence of the sway velocity in the kinematics is not negligible contrary to the case of wheeled mobile robots.

1.3.2.2 Error coordinates

Let $x_d(t)$, $y_d(t)$, $z_d(t)$ denote a given smooth bounded desired trajectory with bounded time derivatives. The objective of this work is to design a controller without incorporating any information regarding the vehicle model such that it tracks the desired trajectory with bounded closed loop signals and prescribed performance (concerning the steady state error and the speed of convergence) despite the presence of exogenous disturbances representing ocean currents and waves. Let us now define the position errors:

$$e_x = x - x_d(t), e_y = y - y_d(t), e_z = z - z_d(t), \quad (1.33)$$

the projected error on the horizontal plane:

$$e_d = \sqrt{e_x^2 + e_y^2} \quad (1.34)$$

as well as the projected on the horizontal plane orientation error:

$$e_o = -\frac{e_x}{e_d} \sin(\psi) + \frac{e_y}{e_d} \cos(\psi) = \sin(\psi_e) \quad (1.35)$$

where ψ_e is the angle measured from the longitudinal axis of the vehicle defined by the 2D vector $[\cos(\psi), \sin(\psi)]^T$ to the vector $\left[-\frac{e_x}{e_d}, -\frac{e_y}{e_d}\right]^T$. Eq. (1.35) can be easily verified if we consider the outer product of the unity vectors $\left[-\frac{e_x}{e_d}, -\frac{e_y}{e_d}\right]^T$ and $[\cos(\psi), \sin(\psi)]^T$ which equals to the sinus of the angle the aforementioned vectors define. Hence, the tracking problem stated above is solved if the projected error on the horizontal plane e_d , the vertical error e_z and the orientation error e_o reduce to zero (i.e., the vehicle is heading to the desired trajectory). However, notice that the orientation error e_o is well-defined only for nonzero values of e_d , since for $e_d = 0$ the angle ψ_e is unidentified. Therefore, in this work, we will design a controller that also guarantees: $e_d(t) > \rho_d > 0, \forall t \geq 0$, with ρ_d an arbitrarily small positive design constant, to avoid the aforementioned singularity issue.

Differentiating (1.34)-(1.35) to derive the kinematics of the underwater vehicle in the error coordinates, we obtain:

$$\begin{aligned} \dot{e}_d &= -u \cos(\psi_e) - v \sin(\psi_e) - (\delta_x(t) - \dot{x}_d(t)) \cos(\psi + \psi_e) \\ &\quad - (\delta_y(t) - \dot{y}_d(t)) \sin(\psi + \psi_e) \end{aligned} \quad (1.36)$$

$$\dot{e}_z = w + \delta_z(t) - \dot{z}_d(t) \quad (1.37)$$

$$\begin{aligned} \dot{e}_o &= -r \cos(\psi_e) + u \frac{e_o \cos(\psi_e)}{e_d} - v \frac{1 - e_o^2}{e_d} + (\delta_x(t) - \dot{x}_d(t)) \frac{\sin(\psi) + e_o \cos(\psi + \psi_e)}{e_d} \\ &\quad - (\delta_y(t) - \dot{y}_d(t)) \frac{\cos(\psi) - e_o \sin(\psi + \psi_e)}{e_d} \end{aligned} \quad (1.38)$$

where the following equalities have been utilized:

$$\begin{aligned} e_x &= -e_d \cos(\psi + \psi_e) \\ e_y &= -e_d \sin(\psi + \psi_e) \end{aligned}$$

Finally, to solve the tracking problem stated above, we assume that the initial projected error on the horizontal plane $e_d(0)$ and orientation heading $\psi_e(0)$ satisfy: a) $e_d(0) > \underline{\rho}_d$ and b) $|\psi_e(0)| < \frac{\pi}{2}$.

1.3.2.3 Control Scheme

Given a smooth bounded desired trajectory $x_d(t)$, $y_d(t)$, $z_d(t)$ with bounded time derivatives, and any initial system configuration satisfying Assumption 1 for an arbitrarily small positive design constant $\underline{\rho}_d$:

I. Kinematic Controller

Select position/orientation performance functions $\rho_d(t)$, $\rho_z(t)$, $\rho_o(t)$ that i) satisfy:

a. $e_d(0) < \rho_d(0)$	$\underline{\rho}_d < \rho_d(t)$	$\underline{\rho}_d < \lim_{t \rightarrow \infty} \rho_d(t)$
b. $ e_z(0) < \rho_z(0)$	$0 < \rho_z(t)$	$0 < \lim_{t \rightarrow \infty} \rho_z(t)$
c. $ e_o(0) < \rho_o(0) < 1$	$0 < \rho_o(t)$	$0 < \lim_{t \rightarrow \infty} \rho_o(t)$

and ii) incorporate the desired performance specifications regarding the steady state error and the speed of convergence, and design the desired velocities:

$$u_d = k_d \ln \left(\frac{1 + \frac{e_d - \frac{\rho_d(t) + \underline{\rho}_d}{2}}{\frac{\rho_d(t) - \underline{\rho}_d}{2}}}{1 - \frac{e_d - \frac{\rho_d(t) + \underline{\rho}_d}{2}}{\frac{\rho_d(t) - \underline{\rho}_d}{2}}} \right), w_d = -k_z \ln \left(\frac{1 + \frac{e_z(t)}{\rho_z(t)}}{1 - \frac{e_z(t)}{\rho_z(t)}} \right), r_d = k_o \ln \left(\frac{1 + \frac{e_o(t)}{\rho_o(t)}}{1 - \frac{e_o(t)}{\rho_o(t)}} \right) \quad (1.39)$$

with positive control gains k_d , k_z , k_o .

II. Dynamic Controller

Select velocity performance functions $\rho_u(t)$, $\rho_w(t)$, $\rho_r(t)$ that satisfy:

a. $ u(0) - u_d(0) < \rho_u(0)$	$0 < \rho_u(t)$	$0 < \lim_{t \rightarrow \infty} \rho_u(t)$
b. $ w(0) - w_d(0) < \rho_w(0)$	$0 < \rho_w(t)$	$0 < \lim_{t \rightarrow \infty} \rho_w(t)$
c. $ r(0) - r_d(0) < \rho_r(0)$	$0 < \rho_r(t)$	$0 < \lim_{t \rightarrow \infty} \rho_r(t)$

and design the external forces in the surge and heave as well as the external torque in yaw as:

$$X = -k_u \ln \left(\frac{1 + \frac{u - u_d}{\rho_u(t)}}{1 - \frac{u - u_d}{\rho_u(t)}} \right), Z = -k_w \ln \left(\frac{1 + \frac{w - w_d}{\rho_w(t)}}{1 - \frac{w - w_d}{\rho_w(t)}} \right), N = -k_r \ln \left(\frac{1 + \frac{r - r_d}{\rho_r(t)}}{1 - \frac{r - r_d}{\rho_r(t)}} \right) \quad (1.40)$$

with positive control gains k_u , k_w , k_r .

1.3.2.4 Experiments

To illustrate the tracking performance and the robustness of the proposed scheme, an experimental procedure was carried out. The experiments took place inside a water tank using a small underwater vehicle.

System Components

The ROV used (VideoRay PRO, VideoRay LLC) is equipped with three thrusters, affecting only the surge, heave and yaw motion. Hence, the vehicle is under-actuated

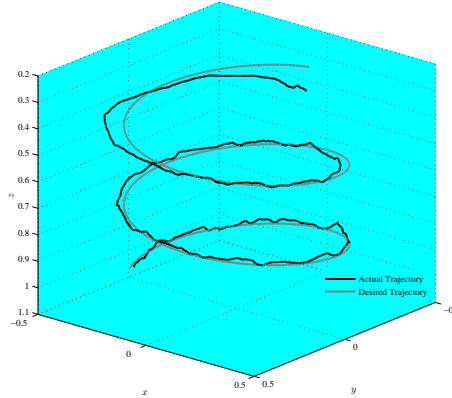


Figure 1.14: The trace along with the desired trajectory.

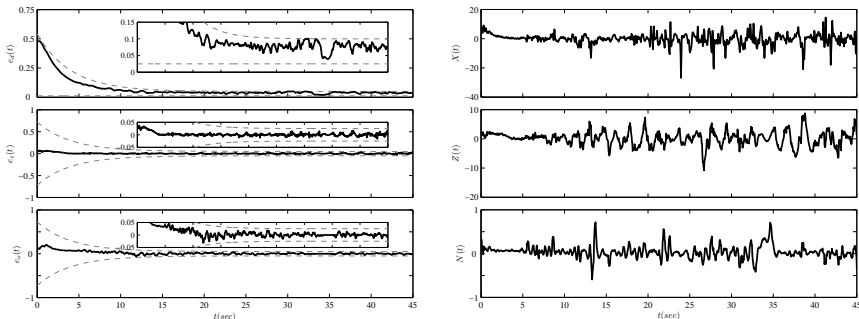
along the sway axis. The angles ϕ , θ and angular velocities p and q are negligible. The ROV is symmetric about x - z plane and close to symmetric about y - z plane. Therefore, we can safely assume that motions in heave, roll and pitch are decoupled [1]. Although the vehicle is not symmetric about x - y plane, heave motion can be considered decoupled from surge and sway because the vehicle is operating at relative low speeds, where coupling effects are considered to be negligible. Thus, the ROV used for the experimental procedure meets the required properties. The vehicle is also equipped with a control unit and a CCD camera. The control unit is connected with a Personal Computer (PC) through a serial communication interface (RS-232). A position sensor (Polhemus, Isotrak) was used as pose feedback sensor for the motion control scheme. The Isotrak tracking system uses electro-magnetic fields to determine the position and orientation of a remote tracker. The Isotrak interfaces to the host computer via RS-232 serial communication at 30 Hz. The Isotrak system consists of a transmitter and a receiver. The transmitter is placed at a fixed position outside the tank and the receiver (tracker) is placed on the vehicle. The system software is implemented in C++. The operating system is Linux.

Results

The ROV starts at rest from initial configuration: $x(0) = 0.15$ m, $y(0) = 0.00$ m, $z(0) = 0.25$ m, $\psi(0) = -120^\circ$ and is requested to track the trajectory: $x_d(t) = -0.4 \sin(0.1\pi t)$, $y_d(t) = -0.4 \cos(0.1\pi t)$, $z_d(t) = 0.3 + 0.015t$, with maximum steady state errors $e_{d_{\max}} = 0.10$, $e_{z_{\max}} = 0.05$, $e_{o_{\max}} = 0.05$ and minimum convergence rate as obtained by the exponential $e^{-0.25t}$. Notice that the aforementioned initial configuration satisfies Assumption 1 for $\rho_d = 0.025$. Hence, we selected the performance functions: $\rho_d(t) = (0.52 - 0.1)e^{-0.25t} + 0.1$, $\rho_z(t) = (0.7 - 0.05)e^{-0.25t} + 0.05$, $\rho_o(t) = (0.7 - 0.05)e^{-0.25t} + 0.05$, $\rho_u(t) = (2 - 0.1)e^{-0.25t} + 0.1$, $\rho_w(t) = (2 - 0.1)e^{-0.25t} + 0.1$, $\rho_r(t) = (2 - 0.1)e^{-0.25t} + 0.1$ and the control gains: $k_d = 0.3$, $k_z = 1$, $k_o = 1$, $k_u = 7.5$, $k_w = 5.0$, $k_r = 0.25$ such that (1.40) produce reasonable control effort. As it was predicted by the theoretical analysis and is actually depicted in Fig. 1.15a, tracking with prescribed performance is successfully achieved with the errors evolv-

ing strictly within the predefined performance bounds, despite the lack of knowledge regarding the ROV dynamic model parameters. The trace of the ROV along with the desired trajectory are illustrated in Fig. 1.14. Additionally, as it is pictured in Fig. 1.15b the required control effort was satisfactorily smooth and did not impose any saturation to the thrusters.

Unfortunately, with the existing setup we were not able to create external disturbances in the form of waves and currents. However, the tether attached to the vehicle, was creating non-trivial external disturbances in the form of random forces and torques while the vehicle was constantly changing configuration during the experiment. As it can be seen from Fig. 1.15a and the overall performance of the controller, these external disturbances were rejected successfully proving thus the efficiency and robustness of the proposed control scheme.



(a) The grey dashed lines indicate the desired performance bounds. The black solid lines indicate the evolution of $e_d(t)$, $e_z(t)$ and $e_o(t)$.

(b) The required control effort along Surge (N), Heave (N) and about Yaw (Nm) during the experiment.

Figure 1.15: Experimental results.

1.3.3 Underactuated Underwater Vehicles - Case II

A six DoFs dynamic model of a torpedo-like AUV is presented in this section and a rigorous formulation of the problem of tracking a desired trajectory is introduced. The vehicle considered in this work is actuated by a force X along its longitudinal axis (surge), by a torque M about its transverse axis (pitch) as well as by a torque N about its vertical axis (yaw). The aforementioned force X and torques M , N define the input control variables of the dynamic system. In this respect, the vehicle is underactuated since only three of its six DoFs are actuated (sway, heave and roll are unactuated).

1.3.3.1 AUV kinematics and dynamics

Consider a neutrally buoyant AUV modeled as a rigid body subject to external forces and torques. Let $\{I\}$ be an inertial coordinate frame and $\{B\}$ a body-fixed coordinate frame with orthonormal axes $\bar{n} = [n_x, n_y, n_z]^T$, $\bar{o} = [o_x, o_y, o_z]^T$, $\bar{t} = [t_x, t_y, t_z]^T$ relatively to $\{I\}$, whose origin O_B is located at the center of mass of the vehicle

that coexists with the center of buoyancy. Further let $\mathbf{p} = [x, y, z]^T$ be the position of O_B in $\{I\}$ and $R = [\bar{n}, \bar{o}, \bar{t}]$ a rotation matrix that describes the orientation of the vehicle. Let $\mathbf{v} = [u, v, w]^T$ be the linear velocity (u, v, w are the longitudinal-surge, transverse-sway and vertical-heave velocities respectively) and $\mathbf{w} = [p, q, r]^T$ be the angular velocity (p, q, r are the angular velocities around the longitudinal-roll, the transverse-pitch and vertical-yaw axis respectively) of O_B w.r.t. to $\{I\}$ expressed in $\{B\}$.

Hence, the kinematic equations of motion for the considered AUV can be written as:

$$\dot{\mathbf{p}} = R\mathbf{v} + \delta_v(t) \quad (1.41)$$

$$\dot{R} = RS(\mathbf{w}) \quad (1.42)$$

where $\delta_v(t) = [\delta_x(t), \delta_y(t), \delta_z(t)]^T$ denotes bounded ocean currents and $S(\mathbf{w}) = \begin{bmatrix} 0 & -r & q \\ r & 0 & -p \\ -q & p & 0 \end{bmatrix}$.

The dynamic equations of motion for the underactuated AUV considered in this work can be written as:

$$m_u \dot{u} = m_v v r - m_w w q + X_u u + X + \delta_u(t) \quad (1.43)$$

$$m_v \dot{v} = m_w w p - m_u u r + Y_v v + \delta_v(t) \quad (1.44)$$

$$m_w \dot{w} = m_u u q - m_v v p + Z_w w + \delta_w(t) \quad (1.45)$$

$$m_p \dot{p} = m_{vw} v w + m_{qr} q r + K_p p + \delta_p(t) \quad (1.46)$$

$$m_q \dot{q} = m_{wu} w u + m_{rp} r p + M_q q + M + \delta_q(t) \quad (1.47)$$

$$m_r \dot{r} = m_{uv} u v + m_{pq} q q + N_r r + N + \delta_r(t) \quad (1.48)$$

where $m_u, m_v, m_w, m_p, m_q, m_r$ denote the AUV's mass/moment of inertia and added mass/moment of inertia terms with $m_{vw} = m_v - m_w, m_{wu} = m_w - m_u, m_{uv} = m_u - m_v, m_{qr} = m_q - m_r, m_{rp} = m_r - m_p, m_{pq} = m_p - m_q$ and $X_u, Y_v, Z_w, K_p, M_q, N_r$ are negative hydrodynamic damping coefficients. Moreover, $\delta_u(t), \delta_v(t), \delta_w(t), \delta_p(t), \delta_q(t), \delta_r(t)$ denote bounded exogenous forces and torques acting on surge, sway, heave, roll, pitch, yaw owing to ocean waves and X, M, N denote the control input force and torques respectively that are applied in order to produce the desired motion of the body fixed frame. Furthermore, notice that there is no control input in the sway, heave and roll equation of motion. Hence, Eqs. (1.44)-(1.46) are uncontrolled making thus (1.41)-(1.48) an underactuated dynamical system. Finally, it should be noted that contrary to the majority of the works in the current AUV literature, where the Euler angles parameterization is mainly employed owing to its physical meaning, our approach, which is based on the rotation matrix parameterization, does not suffer from geometric singularities when the pitch angle approaches $\pm 90^\circ$.

1.3.3.2 Error coordinates

Let $x_d(t), y_d(t), z_d(t)$ denote a smooth, bounded desired trajectory with bounded time derivatives. The objective of this work is to design a robust controller, without

incorporating any information regarding the AUV model, such that it tracks the desired trajectory with bounded closed loop signals and prescribed performance (concerning the steady state error and the speed of convergence) despite the presence of exogenous disturbances representing ocean currents and waves. Let us now define the position error:

$$e_d = \sqrt{e_x^2 + e_y^2 + e_z^2} \quad (1.49)$$

where

$$e_x = x_d(t) - x, e_y = y_d(t) - y, e_z = z_d(t) - z \quad (1.50)$$

as well as the orientation errors:

$$e_o = \frac{e_x}{e_d} o_x + \frac{e_y}{e_d} o_y + \frac{e_z}{e_d} o_z = \cos(\theta_o) \quad (1.51)$$

$$e_t = \frac{e_x}{e_d} t_x + \frac{e_y}{e_d} t_y + \frac{e_z}{e_d} t_z = \cos(\theta_t) \quad (1.52)$$

where θ_o, θ_t are the angles measured from the vector $\bar{e}_d = \left[\frac{e_x}{e_d}, \frac{e_y}{e_d}, \frac{e_z}{e_d} \right]^T$ to the transverse \bar{o} and vertical \bar{t} axis of the AUV respectively. Eqs. (1.51) and (1.52) can be easily verified if we consider the inner product of the unite vector \bar{e}_d with the unite vectors of the transverse \bar{o} and vertical \bar{t} axis respectively, which equals to the cosine of the angle defined by the aforementioned vectors. Hence, the tracking problem stated above is solved if the position error e_d and the orientation errors e_o, e_t reduce to zero (i.e., the AUV is heading to the desired trajectory since in such case the unite vector \bar{e}_d tends to be normal to both the transverse \bar{o} and vertical \bar{t} axis of the AUV and consequently aligned to its longitudinal \bar{n} axis). However, notice that the orientation errors e_o, e_t are well-defined only for nonzero values of e_d , since for $e_d = 0$ the angles θ_o, θ_t are unidentified. Thus, in this work, we will design a controller that further guarantees that $e_d(t) > \rho_d > 0, \forall t \geq 0$ for an arbitrarily small positive design constant ρ_d , to avoid the aforementioned singularity issue.

Differentiating (1.49)-(1.52) and employing (1.41), (1.42) to obtain the kinematics of the AUV in the error coordinates, we arrive at:

$$\dot{e}_d = -u \cos(\theta_n) - v \cos(\theta_o) - w \cos(\theta_t) + \frac{e_x(\dot{x}_d - \delta_x)}{e_d} + \frac{e_y(\dot{y}_d - \delta_y)}{e_d} + \frac{e_z(\dot{z}_d - \delta_z)}{e_d} \quad (1.53)$$

$$\begin{aligned} \dot{e}_o &= -r \cos(\theta_n) + p \cos(\theta_t) + u \frac{\cos(\theta_n) \cos(\theta_o)}{e_d} + (\dot{x}_d - \delta_x) \frac{e_d o_x + e_x \cos(\theta_o)}{e_d^2} - v \frac{\sin^2(\theta_o)}{e_d} \\ &\quad + (\dot{y}_d - \delta_y) \frac{e_d o_y + e_y \cos(\theta_o)}{e_d^2} + w \frac{\cos(\theta_t) \cos(\theta_o)}{e_d} + (\dot{z}_d - \delta_z) \frac{e_d o_z + e_z \cos(\theta_o)}{e_d^2} \end{aligned} \quad (1.54)$$

$$\begin{aligned} \dot{e}_t &= q \cos(\theta_n) - p \cos(\theta_o) + u \frac{\cos(\theta_n) \cos(\theta_t)}{e_d} + (\dot{x}_d - \delta_x) \frac{e_d t_x + e_x \cos(\theta_t)}{e_d^2} + v \frac{\cos(\theta_o) \cos(\theta_t)}{e_d} \\ &\quad + (\dot{y}_d - \delta_y) \frac{e_d t_y + e_y \cos(\theta_t)}{e_d^2} - w \frac{\sin^2(\theta_t)}{e_d} + (\dot{z}_d - \delta_z) \frac{e_d t_z + e_z \cos(\theta_t)}{e_d^2} \end{aligned} \quad (1.55)$$

where the following equality has been utilized:

$$\frac{e_x}{e_d} n_x + \frac{e_y}{e_d} n_y + \frac{e_z}{e_d} n_z = \cos(\theta_n)$$

with θ_n denoting the angle measured from the vector \bar{e}_d to the longitudinal \bar{n} axis of the AUV. Finally, to solve the tracking problem stated above, we assume that the initial position error $e_d(0)$ and orientation heading $\theta_n(0)$ satisfy: a) $e_d(0) > \underline{\rho}_d$ and b) $|\theta_n(0)| < \frac{\pi}{2}$.

1.3.3.3 Control Scheme

Given a smooth, bounded desired trajectory $x_d(t)$, $y_d(t)$, $z_d(t)$ with bounded time derivatives, and any initial system configuration satisfying Assumption 1 for an arbitrarily small positive design constant $\underline{\rho}_d$:

I. Kinematic Controller

Select position/orientation performance functions $\rho_d(t)$, $\rho_o(t)$, $\rho_t(t)$ that i) satisfy:

a. $e_d(0) < \rho_d(0)$	$\underline{\rho}_d < \rho_d(t)$	$\underline{\rho}_d < \lim_{t \rightarrow \infty} \rho_d(t)$
b. $ e_o(0) < \rho_o(0) < 1$	$0 < \rho_o(t)$	$0 < \lim_{t \rightarrow \infty} \rho_o(t)$
c. $ e_t(0) < \rho_t(0) < 1$	$0 < \rho_t(t)$	$0 < \lim_{t \rightarrow \infty} \rho_t(t)$
d. $\rho_o^2(t) + \rho_t^2(t) \leq \bar{\rho} < 1, \forall t \geq 0$		

for a positive constant $\bar{\rho} < 1$ and ii) incorporate the desired performance specifications regarding the steady state error and the speed of convergence. Subsequently, design the desired velocities:

$$u_d = k_d \ln \left(\frac{1 + \frac{e_d - \frac{\rho_d(t) + \rho_d}{2}}{\frac{\rho_d(t) - \underline{\rho}_d}{2}}}{1 - \frac{e_d - \frac{\rho_d(t) + \rho_d}{2}}{\frac{\rho_d(t) - \underline{\rho}_d}{2}}} \right), q_d = -k_t \ln \left(\frac{1 + \frac{e_t}{\rho_t(t)}}{1 - \frac{e_t}{\rho_t(t)}} \right), r_d = k_o \ln \left(\frac{1 + \frac{e_o(t)}{\rho_o(t)}}{1 - \frac{e_o(t)}{\rho_o(t)}} \right) \quad (1.56)$$

with positive control gains k_d , k_o , k_t .

II. Dynamic Controller

Select velocity performance functions $\rho_u(t)$, $\rho_q(t)$, $\rho_r(t)$ that satisfy:

a. $ u(0) - u_d(0) < \rho_u(0)$	$0 < \rho_u(t)$	$0 < \lim_{t \rightarrow \infty} \rho_u(t)$
b. $ q(0) - q_d(0) < \rho_q(0)$	$0 < \rho_q(t)$	$0 < \lim_{t \rightarrow \infty} \rho_q(t)$
c. $ r(0) - r_d(0) < \rho_r(0)$	$0 < \rho_r(t)$	$0 < \lim_{t \rightarrow \infty} \rho_r(t)$

and design the external force in the surge as well as the external torques in pitch and yaw as:

$$X = -k_u \ln \left(\frac{1 + \frac{u - u_d}{\rho_u(t)}}{1 - \frac{u - u_d}{\rho_u(t)}} \right), M = -k_q \ln \left(\frac{1 + \frac{q - q_d}{\rho_q(t)}}{1 - \frac{q - q_d}{\rho_q(t)}} \right), N = -k_r \ln \left(\frac{1 + \frac{r - r_d}{\rho_r(t)}}{1 - \frac{r - r_d}{\rho_r(t)}} \right) \quad (1.57)$$

with positive control gains k_u , k_q , k_r .

1.3.3.4 Simulation Results

To illustrate the tracking performance and the robustness of the proposed scheme against external disturbances representing ocean currents and waves, two simulation

studies were carried out on a 6 DOF torpedo-like AUV actuated in surge, pitch and yaw. The vehicle dynamic model used in the simulation can be found in [20]. The AUV starts at rest from initial configuration: $x(0) = -65$ m, $y(0) = -15$ m, $z(0) = 5$ m, $R(0) = [0 \ 1 \ 0; 1 \ 0 \ 0; 0 \ 0 \ 1]$ and is requested to track the trajectory: $x_d(t) = -50 \cos(0.02\pi t)$ m, $y_d(t) = 0.15\pi t$ m, $z_d(t) = 50 \sin(0.02\pi t)$ m, with maximum steady state errors $e_{d\max} = 0.1$, $e_{o\max} = 0.01$, $e_{t\max} = 0.01$ and minimum convergence rate as obtained by the exponentials $e^{-0.1t}$, e^{-t} and e^{-t} . Notice that the aforementioned initial configuration satisfies Assumption 1 for $\rho_d = 0.05$. Hence, following Subsection IV-A, we select the performance functions: $\rho_d(t) = (40 - 0.1)e^{-0.1t} + 0.1$, $\rho_o(t) = (0.45 - 0.01)e^{-t} + 0.01$, $\rho_t(t) = (0.45 - 0.01)e^{-t} + 0.01$, $\rho_u(t) = (2 - 0.1)e^{-t} + 0.1$, $\rho_q(t) = (2 - 0.1)e^{-t} + 0.1$, $\rho_r(t) = (2 - 0.1)e^{-t} + 0.1$ and the control gains: $k_d = 5$, $k_o = 1$, $k_t = 1$, $k_u = 500$, $k_q = 100$, $k_r = 100$ such that (1.57) yield reasonable control effort.

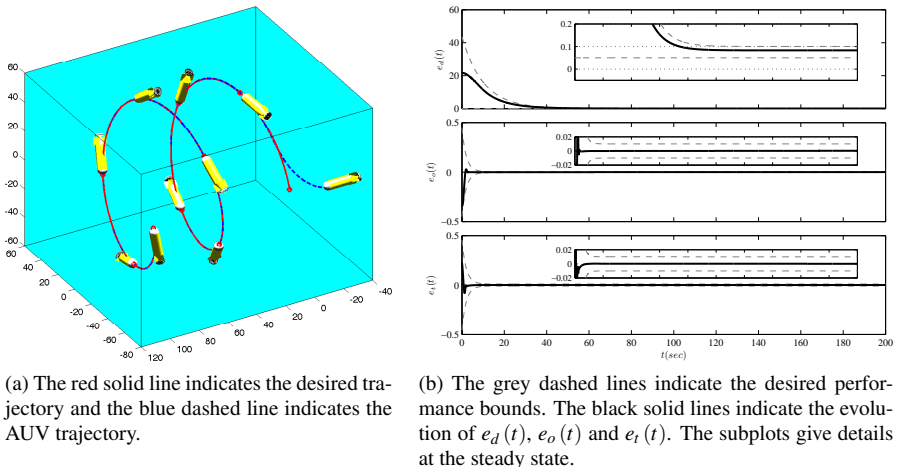
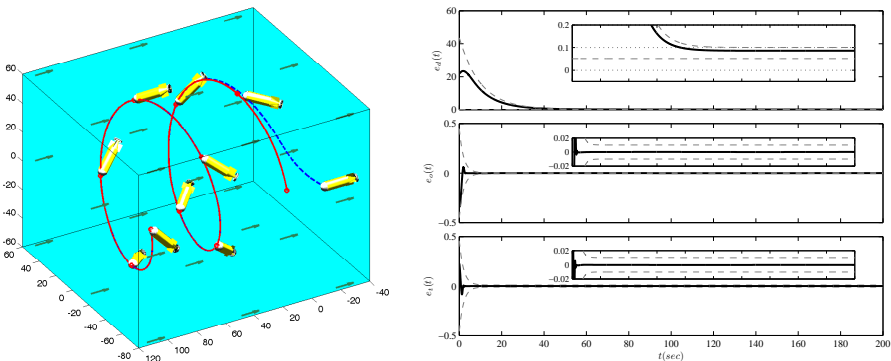


Figure 1.16: Disturbance-free case. (a) Trajectory tracking in 3D space. (b) Tracking error evolution.

In the first study, we considered a disturbance-free case. On the contrary, the second study captured the case where the ocean current is $d_x(t) = 0$, $d_y(t) = -2.5$, $d_z(t) = 0$ and the wave terms include three sinusoids with amplitude and frequency equally distributed in $[0.1, 1]$ and $[0.01, 0.1]$ respectively. The trajectory tracking is shown in Figs. 1.16a and 1.17a. The output error evolution along with the performance bounds are pictured in Figs. 1.16b and 1.17b. As it was predicted, tracking with prescribed performance is achieved despite the presence of external disturbances and the lack of knowledge of the AUV model parameters.



(a) The red solid line indicates the desired trajectory and the blue dashed line indicates the AUV trajectory.

(b) The grey dashed lines indicate the desired performance bounds. The black solid lines indicate the evolution of $e_d(t)$, $e_o(t)$ and $e_t(t)$. The subplots give details at the steady state.

Figure 1.17: Case of ocean currents and waves. (a) Trajectory tracking in 3D space. (b) Tracking error evolution.

References

- [1] Fossen TI. Guidance and Control of Ocean Vehicles. Chichester, U.K.: Wiley; 1994.
- [2] Lawton JRT, Beard RW, Young BJ. A decentralized approach to formation maneuvers. *IEEE Transactions on Robotics and Automation*. 2003;19(6):933–941.
- [3] Repoulias F, Papadopoulos E. Planar trajectory planning and tracking control design for underactuated AUVs. *Ocean Engineering*. 2007;34(11-12):1650–1667.
- [4] Aguiar AP, Hespanha JP. Trajectory-tracking and path-following of underactuated autonomous vehicles with parametric modeling uncertainty. *IEEE Transactions on Automatic Control*. 2007;52(8):1362–1379.
- [5] Santhakumar M, Asokan T. Investigations on the hybrid tracking control of an underactuated autonomous underwater robot. *Advanced Robotics*. 2010;24(11):1529–1556.
- [6] Allgöwer F, Findeisen R, Nagy ZK. Nonlinear model predictive control: From theory to application. *the Chinese Institute of Chemical Engineers*. 2004;35(3):299–315.
- [7] Medagoda L, Williams SB. Model predictive control of an autonomous underwater vehicle in an in situ estimated water current profile. Program Book - OCEANS 2012 MTS/IEEE Yeosu: The Living Ocean and Coast - Diversity of Resources and Sustainable Activities. 2012;

- [8] Fernandez DC, Hollinger GA. Model Predictive Control for Underwater Robots in Ocean Waves. *IEEE Robotics and Automation Letters*. 2017;2(1):88–95.
- [9] Jagtap P, Raut P, Kumar P, et al. Control of autonomous underwater vehicle using reduced order model predictive control in three dimensional space. *IFAC-PapersOnLine*. 2016;49(1):772–777.
- [10] Heshmati-Alamdar S, Eqtami A, Karras GC, et al. A self-triggered visual servoing model predictive control scheme for under-actuated underwater robotic vehicles. *Proceedings - IEEE International Conference on Robotics and Automation*. 2014;p. 3826–3831.
- [11] Naitonal HF RADAR network - surface currents;. Available from: <http://cordc.ucsd.edu/projects/mapping/maps/>.
- [12] Smith RN, Chao Y, Li PP, et al. Planning and implementing trajectories for autonomous underwater vehicles to track evolving ocean processes based on predictions from a regional ocean model. *International Journal of Robotics Research*. 2010;29(12):1475–1497.
- [13] Aguiar AP, Pascoal AM. Dynamic positioning and way-point tracking of underactuated AUVs in the presence of ocean currents. *International Journal of Control*. 2007;80(7):1092–1108.
- [14] Fossen TI. *Guidance and control of ocean vehicles*. Wiley, New York. 1994;
- [15] Asouti VG, Trompoukis XS, Kampolis IC, et al. Unsteady CFD computations using vertex-centered finite volumes for unstructured grids on Graphics Processing Units. *International Journal for Numerical Methods in Fluids*. 2011;67(2):232–246.
- [16] Koditschek DE, Rimon E. Robot navigation functions on manifolds with boundary. *Advances in Applied Mathematics*. 1990;11(4):412–442.
- [17] Garrido-Jurado S, noz Salinas RM, Madrid-Cuevas FJ, et al. Automatic generation and detection of highly reliable fiducial markers under occlusion. *Pattern Recognition*. 2014;47(6):2280 – 2292.
- [18] Marantos P, Koveos Y, Kyriakopoulos KJ. UAV State Estimation Using Adaptive Complementary Filters. *IEEE Transactions on Control Systems Technology*. 2016;24(4):1214–1226.
- [19] Quigley M, Gerkey B, Conley K, et al. ROS: an open-source Robot Operating System. In: Proc. of the IEEE Intl. Conf. on Robotics and Automation (ICRA) Workshop on Open Source Robotics. Kobe, Japan; 2009. .
- [20] Pettersen KY, Egeland O. Time-varying exponential stabilization of the position and attitude of an underactuated autonomous underwater vehicle. *IEEE Transactions on Automatic Control*. 1999;44(1):112–115.